Loopy Lévy flights enhance tracer diffusion in active suspensions

Kiyoshi Kanazawa*

Faculty of Engineering, Information and Systems,

University of Tsukuba, Tennodai, Tsukuba, Ibaraki 305-8577, Japan

Tomohiko G. Sano

Flexible Structures Laboratory, Institute of Mechanical Engineering,

École polytechnique fédérale de Lausanne, Lausanne, CH-1015, Switzerland.

Andrea Cairoli

Department of Bioengineering, Imperial College London, London SW7 2AZ, UK

Adrian Baule

School of Mathematical Sciences, Queen Mary University of London, London E1 4NS, UK

(Dated: December 15, 2019)

* kiyoshi@sk.tsukuba.ac.jp

Brownian motion is widely used as a paradigmatic model of diffusion in equilibrium media throughout the physical, chemical, and biological sciences. However, many real world systems are intrinsically out-of-equilibrium due to the energy-dissipating active processes underlying their mechanical and dynamical features [1]. The diffusion process followed by a passive tracer in prototypical active media such as suspensions of active colloids or swimming microorganisms [2] indeed differs significantly from Brownian motion, manifest in a greatly enhanced diffusion coefficient [3–10] and non-Gaussian statistics of the tracer displacements [6, 9, 10]. While such characteristic features have been extensively observed in experiments, there is so far no comprehensive theory explaining how they emerge from the microscopic dynamics. Here we develop a theoretical framework to coarse-grain the hydrodynamic interactions between the tracer and the active swimmers, which shows that the tracer follows a non-Markovian coloured Poisson process accounting for all empirical observations. The theory predicts in particular a long-lived Lévy flight regime [11] of the tracer motion with a non-monotonic crossover between two different power-law exponents. The duration of this regime can be tuned by the swimmer density, thus suggesting that the optimal foraging strategy of swimming microorganisms might crucially depend on the density in order to exploit the Lévy flights of nutrients [12]. Our framework can be applied to address important conceptual questions, such as the thermodynamics of active systems [13], and practical ones, such as the interaction of swimming microorganisms with nutrients and other small particles like degraded plastic [14] and the design of artificial nanoscale machines [15].

A passive tracer immersed in a fluid at equilibrium moves randomly due to its collisions with the surrounding fluid molecules. Understanding how the stochastic process of the tracer relates to the statistical mechanics of the surrounding fluid, as accomplished in the seminal works by Einstein, Smoluchowski, and Langevin [16], has provided deep insight into the connection between molecular transport and equilibrium thermodynamics, which has been widely exploited to describe soft matter and other complex physical systems [17]. However, when either artificial self-propelled colloids or biological swimming micro-organisms, such as bacteria like *Escherichia coli* or algae like *Volvox* and *Chlamydomonas reinhardtii* [2], are also suspended, the diffusion of the tracer changes dramatically due to the active stirring of the

fluid exerted by the swimmers. Indeed, the tracer exhibits empirically the following unique features that can no longer be explained as a Brownian motion: (i) the tracer exhibits loopy trajectories [4, 8, 9]; (ii) its mean square displacement (MSD) exhibits a crossover between superdiffusion with characteristic scaling t^α ($1 < \alpha \leq 2$) for short times and normal diffusion ($\alpha = 1$) for long times, where the effective diffusion coefficient D_e is greatly enhanced compared with the equilibrium coefficient D_0: $D_\mathrm{e} = D_0 + B\rho v_\mathrm{A}$, with the density of swimmers ρ, characteristic swimming velocity v_A, and a system-dependent parameter B [3–5, 7–9]; (iii) the probability density function (PDF) $P_{\Delta t}$ of tracer displacements in a given time interval Δt exhibits strong non-Gaussian features manifest as power-law tails [6, 10]; (iv) $P_{\Delta t}$ eventually reverts to a Gaussian shape for large Δt [9, 10]; (v) the associated non-Gaussian parameter (NGP) exhibits a characteristic scaling Δt^{-1} for large times [10].

Developing a single theory that captures all features (i)–(v) has been a major challenge. While the loop-like motion (i) results from an individual scattering event of the tracer in the dipolar flow field of a single swimmer [7, 18, 19], and the linear form of D_e (ii) has been explained phenomenologically based on the active flux ρv_A of the swimmers [5, 7, 8, 19, 20], the statistical observations (iii)–(v) could so far not be explained consistently. The power-law tails in $P_{\Delta t}$ and their convergence to Gaussian scaling for large Δt, which is expected based on central limit theorem (CLT) arguments [21, 22], have been reproduced in [10, 23, 24] assuming a static force distribution akin to the Holtsmark theory of gravitating particles [25] (see Supplementary Information (SI) Sec. VI C for a review). However, this approach neglects any dynamics of the swimmers and is thus not sufficient to capture the enhanced diffusion observed in experiments [3–10]. Here we present a derivation of the stochastic process underlying the tracer diffusion from the microscopic hydrodynamic interactions. The resulting process is valid at all timescales and captures all characteristic features (i)–(v).

We consider a three-dimensional system composed of m active particles (swimmers) and a passive tracer suspended in a viscous fluid inside a cubic box (Fig. 1a). The swimmers are assumed self-propelled moving unidirectionally with constant velocity v_A [26]. In general, the dynamics of such a multi-particle system with long-range hydrodynamic interactions is analytically intractable. However, suspensions of micro-organisms often considered in experiments are characterized by (a) low Reynolds number swimming and (b) a low density of swimmers (dilute condition, see below). In particular the dilute condition (b) allows us to neglect the mutual hydrodynamic interactions of the swimmers [27], leading to the

overdamped equations of motion:

$$\frac{\mathrm{d}\mathbf{x}_i}{\mathrm{d}t} = v_\mathrm{A}\mathbf{n}_i, \qquad \Gamma\frac{\mathrm{d}\mathbf{X}}{\mathrm{d}t} = \sum_{i=1}^{m}\mathbf{F}(\mathbf{x}_i - \mathbf{X}, \mathbf{n}_i), \tag{1}$$

where $\mathbf{F}$ is the force on the tracer generated by a single swimmer and Γ is a viscous coefficient for the passive particle. In Eq. (1), $\mathbf{x}_i(t)$ and $\mathbf{X}(t)$ denote the positions of the i-th active particle and the passive particle, respectively, and the unit vector $\mathbf{n}_i$ specifies the swimming direction.

The low Reynolds number condition (a) further yields a closed form expression for $\mathbf{F}$ as the solution of the Stokes equation. For force- and torque-free swimmers, the leading-order term in a far-field expansion is a dipole force [26]

$$\mathbf{F}(\mathbf{r}_i, \mathbf{n}_i) \approx \frac{p}{r_i^2}\left[3\frac{(\mathbf{n}_i\cdot\mathbf{r}_i)^2}{r_i^2} - 1\right]\frac{\mathbf{r}_i}{r_i}, \qquad r_i > d \tag{2}$$

with the difference vector $\mathbf{r}_i = \mathbf{x}_i - \mathbf{X}$ and the system specific cut-off d, which separates the far–flow field from any near–flow field hydrodynamic contributions and hard-core interactions. The dipole strength parameter p specifies the universal features of the far-flow hydrodynamic field [26]: $p < 0$ denotes *pusher* swimmers whose flow lines are oriented outward along the direction of its velocity vector and inward laterally (e.g., *E. coli* [26]); $p > 0$ denotes instead *puller* swimmers whose flow lines are oriented in the opposite directions (e.g., *C. reinhardtii* [26]). For $r_i \leq d$ the interaction force $\mathbf{F}$ is not universal but system-specific. Nevertheless, all swimmer–tracer interactions in this regime can be accurately captured using arguments based on the CLT, which do not require a detailed form of $\mathbf{F}$. Therefore, we set for simplicity $\mathbf{F} = 0$ in this regime [10]. The model has one further length parameter $b^* \equiv \sqrt{|p|/(\Gamma v_\mathrm{A})}$, which can be related to the typical length scale of the swimmers [26]. All these parameters can be determined experimentally: for *E. coli* $v_\mathrm{A} \simeq 30\mu$m/s, $d \simeq 6\,\mu$m and $b^* \simeq 2\,\mu$m [5, 27]; for *C. reinhardtii* $v_\mathrm{A} \simeq 100\mu$m/s, $d \simeq 35\,\mu$m and $b^* \simeq 8\,\mu$m [10, 23, 24, 28]; both are satisfying $d \geq b^*$.

Simulations of Eqs. (1,2) under the dilute condition reproduce all features (i)–(v) (see Fig. 1b, Fig. 3, and Supplementary Video). Crucially, the time-series of the force exerted on the tracer highlights that its dynamics can be resolved as a sequence of individual scattering events, where only two–body tracer–swimmer interactions are relevant (Fig. 2a). In the kinetic theory of gases, a similar description in terms of binary scattering events is ensured by requiring $\rho r_\mathrm{c}^3 \ll 1$, where r_c denotes the range of the interparticle interaction force. Even

though for long-range hydrodynamic forces an interaction range cannot be well defined, we identify in our system r_c as the maximum of the characteristic length scales available: $r_c \equiv \max\{d, b^*\} = d$. The motivation behind this definition of r_c is two-fold. Firstly, the dilute condition $\rho d^3 \ll 1$ is indeed realized in experiments that exhibit the features (i)–(v) (e.g., $\rho d^3 \approx 0.15$ in [10] and $\rho d^3 \approx 0.10$ in [5]). Secondly, this parameter regime allows for a self-consistent description of the tracer dynamics, in which the dipole interaction governs the displacement statistics on short and intermediate time scales, while the statistics for longer times reverts to a Gaussian due to the CLT, as follows.

In a dilute system defined this way, at every instant in time, swimmers on average have $b \gg d$, where b is the impact parameter of a binary swimmer–tracer interaction (see Fig. 1c). The tracer statistics will then be governed by three distinct dynamical regimes: (1.) For short times $\Delta t \ll \tau_H \equiv b^*/v_A$, with τ_H the timescale below which the motion of the swimmers is effectively negligible, the tracer experiences static long-range forces as in the Holtsmark theory [25] ("Holtsmark regime"). (2.) For times $\tau_H \ll \Delta t \ll \tau_C$, the tracer is displaced by the moving swimmers in a sequence of binary "scatterings" governed by the far-flow field interaction force (2) ("scattering regime"). The time scale $\tau_C \equiv 1/(\rho v_A \pi d^2)$ (see Fig. 1c) thus estimates the time necessary for a swimmer to come close enough to the tracer to interact via hard-core and near-field hydrodynamic interactions. (3.) For $\Delta t \gg \tau_C$, the tracer is displaced by an accumulation of these "collisions" with the swimmers such that the CLT applies ("CLT regime").

Remarkably, these three regimes are captured by a coarse-grained description of the tracer dynamics in terms of the Langevin equation

$$\Gamma \frac{\mathrm{d}\mathbf{X}}{\mathrm{d}t} = \sum_{i=1}^{N(t)} \mathbf{f}_{\mathbf{b_i}}(t - \tau_i), \tag{3}$$

where $N(t)$ counts the number of scattering events up to t and $\mathbf{f_b}(t)$ is the force shape function (FSF) describing the force exerted on the tracer during each scattering. The FSF is centred at the scattering time point τ_i, which is set by the condition $\mathbf{n}_i \cdot \mathbf{r}_i = 0$ for the i-th swimmer. The transition from the fully deterministic dynamics of Eqs. (1, 2) to a stochastic description by Eq. (3) is realised by assuming $N(t)$ to be a Poisson process with intensity $\lambda(\mathbf{b})$, whose functional form can be determined from the microscopic dynamics assuming a uniform distribution of swimmers in the box and an isotropic distribution of swimming directions (see SI Sec. II A). The FSF $\mathbf{f_b}(t)$ is characterized by the impact parameter and

injection angles (combined as $\mathbf{b}$; see Fig. 2b) and is obtained in analytical form by solving the binary swimmer–tracer scattering problem. Remarkably, for $b \gg b^*$ an analytical approximation of the FSF can be obtained using a Picard iteration up to 2nd order and subsequent Taylor expansion (see SI Sec. II B–D), which is in very good agreement with numerics (Fig. 2c). The total intensity of the process diverges in the large system size limit because $\lambda(\mathbf{b})\mathrm{d}\mathbf{b} \propto b$ such that $\lim_{L\to\infty} \int \mathrm{d}\mathbf{b}\lambda(\mathbf{b}) = \infty$. Consequently, $\mathbf{X}(t)$ is a coloured Poisson process with infinite intensity, a generalization of the Campbell process [29]. Rather than being unphysical, this infinite intensity is a physical consequence of the long-range hydrodynamic interactions, which cause an infinite number of small scatterings at arbitrarily large distances.

From Eq. (3) we calculate the statistics of the tracer displacement in the x-direction $\Delta X \equiv \mathbf{e}_x \cdot [\mathbf{X}(t+\Delta t) - \mathbf{X}(t)]$, which is typically measured in experiments [4, 6, 9, 10]. Using functional techniques (see SI Sec. III), we derive the displacement PDF $P_{\Delta t}(|\Delta X|)$ and obtain its scaling behaviours in the regimes (1.)–(3.) as

$$P_{\Delta t}(|\Delta X|) \propto \begin{cases} |\Delta X|^{-\alpha_\mathrm{H}} & (\Delta t \ll \tau_\mathrm{H}) \\ |\Delta X|^{-\alpha_\mathrm{S}} & (\tau_\mathrm{H} \ll \Delta t \ll \tau_\mathrm{C}) \\ e^{-\Delta X^2/(2\sigma^2)} & (\tau_\mathrm{C} \ll \Delta t) \end{cases} \tag{4}$$

with power-law exponents $\alpha_\mathrm{H} = 5/2$, $\alpha_\mathrm{S} = 5/3$ and a positive constant σ that depends on d. For finite d a truncation appears in the power-law tails, which is realistic because any physical system must accommodate finite cutoffs [30].

The Holtsmark regime (1.) yields the same scaling behaviour $|\Delta X|^{-\alpha_\mathrm{H}}$ found in the approaches [10, 23, 24] considering static swimmers. For $\Delta t \gtrsim \tau_\mathrm{H}$, these theories are not applicable because the rearrangements of the active swimmers are no longer negligible. Taking into account the scatterings from moving swimmers, the process (3) is non-Markovian. Nevertheless, in the scattering regime (2.), the description becomes effectively Markovian as the FSF can be approximated as a Dirac δ-function (see SI Sec. II). In this regime the coloured Poisson model (3) is equivalent to a compound Poisson process with jump-length distribution prescribed as a power law $\propto |\Delta X|^{-\alpha_\mathrm{S}}$ with a finite cutoff. Our results thus suggest that the celebrated Lévy flight model [11] holds as an approximate description of the tracer dynamics at this timescale. The Lévy flight is a generalization of the standard random walk model to power-law distributed jump sizes, which can capture long jumps in a

single time-step (see SI Sec. IV). If confirmed experimentally, our framework would provide the first validation of this model from a physical microscopic dynamics. In the collision regime (3.), collisions become dominant over scatterings. Since collisional impact has a finite cutoff, the accumulation of a sufficient number of collisions leads to the Gaussian tail as a consequence of the CLT. We note that the detailed form of $\mathbf{F}$ in Eq. (1) for $r_i \leq d$ is renormalized into the variance σ^2.

Using the exact expression for $P_{\Delta t}$ (see SI, Eq. (S40)), the tracer MSD for different swimmer densities is predicted to collapse onto a universal curve upon rescaling by $1/(\rho b^{*5})$, which reveals a crossover from ballistic motion $\propto \rho v_{\mathrm{A}}^2 \Delta t^2$ at short timescales to normal diffusion $\propto \rho v_{\mathrm{A}} \Delta t$ at longer ones (see SI Sec. III A). Likewise, the NGP is predicted to exhibit the scaling $\mathrm{NGP}(\Delta t) \propto (\rho v_{\mathrm{A}})^{-1} \Delta t^{-1}$ upon rescaling by ρb^{*3} (see SI Sec. III B). Eq. (3) thus not only predicts the enhanced diffusion at all time scales but also captures quantitatively the linear dependence of the diffusion coefficient D_{e} on the active flux ρv_{A} as well as the scaling behaviour of the NGP, consistent with experimental observations [3–5, 7–10]. The striking non-monotonic behaviour of the scaling exponents of $P_{\Delta t}$ as predicted by Eq. (4), as well as the data collapse and the scalings for both the MSD and NGP are confirmed in simulations (see Fig. 3).

Our theory can be extended to incorporate thermal fluctuations and more general hydrodynamic forces in arbitrary dimensions. Under thermal noise, the scaling predictions Eq. (4) and that of the NGP are preserved, while the MSD is shifted by a term $2D_0\Delta t$, with $D_0 = k_{\mathrm{B}}T/\Gamma$ and T the temperature of the bath (see SI Secs. III A and B). Interestingly, the data collapse for both the MSD and the NGP no longer holds in this case. Therefore, the presence of data collapse can be probed as a footprint of the relevance of thermal fluctuations on the tracer dynamics. Moreover, our analysis shows that while α_{H} is universally determined by the leading power-law exponent of the hydrodynamic interaction force, n_{H}, as $\alpha_{\mathrm{H}} = 1 + D/n_{\mathrm{H}}$ in D dimensions, the exponent α_{S} depends crucially on the details of the force law (see SI Sec. III C). We find $\alpha_{\mathrm{S}} = 1 + (D-1)/n_{\mathrm{S}}$, where the exponent n_{S} is related to the net tracer displacement during a scattering event and is thus determined by the geometry of particle loops.

Over several magnitudes in time, the tracer is characterized by a linear-in-time MSD with non-Gaussian displacement statistics, an example of "Brownian yet non-Gaussian" diffusion widely observed in non-equilibrium systems [31]. While this behaviour poses considerable

challenges already for purely phenomenological modelling approaches [32], it is here fully captured by the process (3) that is derived from the microscopic dynamics. Moreover, our results pose interesting biological questions on the possible foraging behaviour of real swimming micro-organisms like *C. reinhardtii*. The power-law tail in Eq. (4) persists for longer timescales when the swimmer density ρ decreases, because $\tau_{\rm C} \propto 1/\rho$. Since Lévy flights increase encounter probabilities in stochastic search [12, 33, 34], our results suggest that the foraging strategy of swimming micro-organisms might depend on ρ: for large ρ the Gaussian (spatially localized) displacements of nutrients make an active search like intermittent Lévy-Brownian strategies [35] suitable. Conversely, at low ρ the nutrients exhibit large power-law distributed displacements, such that it might be advantageous for the forager to simply wait for a nutrient to come close. Finally, we remark that superimposing additional force fields such as electric or magnetic forces can be treated within our framework in full analogy to hydrodynamic interactions, which would allow the theoretical investigation of mechanisms to control and exploit enhanced diffusion.

[1] Needleman, D. & Dogic, Z. Active matter at the interface between materials science and cell biology. *Nat. Rev. Mat.* **2**, 17048 (2017).

[2] Koch, D. L. & Subramanian, G. Collective hydrodynamics of swimming microorganisms: Living fluids. *Annu. Rev. Fluid Mech.* **43**, 637–659 (2011).

[3] Wu, X.-L. & Libchaber, A. Particle diffusion in a quasi-two-dimensional bacterial bath. *Phys. Rev. Lett.* **84**, 3017 (2000).

[4] Leptos, K. C., Guasto, J. S., Gollub, J. P., Pesci, A. I. & Goldstein, R. E. Dynamics of enhanced tracer diffusion in suspensions of swimming eukaryotic microorganisms. *Phys. Rev. Lett.* **103**, 198103 (2009).

[5] Miño, G. *et al.* Enhanced diffusion due to active swimmers at a solid surface. *Phys. Rev. Lett.* **106**, 048102 (2011).

[6] Kurtuldu, H., Guasto, J. S., Johnson, K. A. & Gollub, J. P. Enhancement of biomixing by swimming algal cells in two-dimensional films. *Proc. Natl. Acad. Sci.* **108**, 10391–10395 (2011).

[7] Mino, G. L., Dunstan, J., Rousselet, A., Clément, E. & Soto, R. Induced diffusion of tracers

in a bacterial suspension: theory and experiments. *J. Fluid Mech.* **729**, 423–444 (2013).

[8] Jepson, A., Martinez, V. A., Schwarz-Linek, J., Morozov, A. & Poon, W. C. K. Enhanced diffusion of nonswimmers in a three-dimensional bath of motile bacteria. *Phys. Rev. E* **88**, 041002 (2013).

[9] Jeanneret, R., Pushkin, D. O., Kantsler, V. & Polin, M. Entrainment dominates the interaction of microalgae with micron-sized objects. *Nat. Commun.* **7**, 12518 (2016).

[10] Kurihara, T., Aridome, M., Ayade, H., Zaid, I. & Mizuno, D. Non-Gaussian limit fluctuations in active swimmer suspensions. *Phys. Rev. E* **95**, 030601 (2017).

[11] Hughes, B. D., Shlesinger, M. F. & Montroll, E. W. Random walks with self-similar clusters. *Proc. Natl. Acad. Sci.* **78**, 3287–3291 (1981).

[12] Bartumeus, F., Catalan, J., Fulco, U., Lyra, M. & Viswanathan, G. Optimizing the encounter rate in biological interactions: Lévy versus Brownian strategies. *Phys. Rev. Lett.* **88**, 097901 (2002).

[13] Kanazawa, K., Sano, T. G., Sagawa, T. & Hayakawa, H. Minimal model of stochastic athermal systems: Origin of non-Gaussian noise. *Phys. Rev. Lett.* **114**, 090601 (2015).

[14] Goldstein, R. E. Green algae as model organisms for biological fluid dynamics. *Annu. Rev. Fluid Mech.* **47**, 343–375 (2015).

[15] Bechinger, C. *et al.* Active particles in complex and crowded environments. *Rev. Mod. Phys.* **88**, 045006 (2016).

[16] Gardiner, C. W. *Stochastic methods. A handbook for the Natural and social sciences* (Springer-Verlag, Berlin, 2009).

[17] Coffey, W. T. & Kalmykov, Y. P. *The Langevin equation: with applications to stochastic problems in physics, chemistry and electrical engineering* (World Scientific, 2004).

[18] Dunkel, J., Putz, V. B., Zaid, I. M. & Yeomans, J. M. Swimmer-tracer scattering at low Reynolds number. *Soft Matter* **6**, 4268–4276 (2010).

[19] Lin, Z., Thiffeault, J.-L. & Childress, S. Stirring by squirmers. *J. Fluid Mech.* **669**, 167–177 (2011).

[20] Morozov, A. & Marenduzzo, D. Enhanced diffusion of tracer particles in dilute bacterial suspensions. *Soft Matter* **10**, 2748–2758 (2014).

[21] Pushkin, D. O. & Yeomans, J. M. Fluid mixing by curved trajectories of microswimmers. *Phys. Rev. Lett.* **111**, 188101 (2013).

[22] Thiffeault, J.-L. Distribution of particle displacements due to swimming microorganisms. *Phys. Rev. E* **92**, 023023 (2015).

[23] Zaid, I. M., Dunkel, J. & Yeomans, J. M. Lévy fluctuations and mixing in dilute suspensions of algae and bacteria. *J. Royal Soc. Interface* **8**, 1314–1331 (2011).

[24] Zaid, I. & Mizuno, D. Analytical limit distributions from random power-law interactions. *Phys. Rev. Lett.* **117**, 030602 (2016).

[25] Holtsmark, J. Über die Verbreiterung von Spektrallinien. *Ann. Phys. (Berl.)* **363**, 577–630 (1919).

[26] Lauga, E. & Powers, T. R. The hydrodynamics of swimming microorganisms. *Rep. Prog. Phys.* **72**, 096601 (2009).

[27] Drescher, K., Dunkel, J., Cisneros, L. H., Ganguly, S. & Goldstein, R. E. Fluid dynamics and noise in bacterial cell–cell and cell–surface scattering. *Proc. Natl. Acad. Sci.* **108**, 10940–10945 (2011).

[28] Drescher, K., Goldstein, R. E., Michel, N., Polin, M. & Tuval, I. Direct measurement of the flow field around swimming microorganisms. *Phys. Rev. Lett.* **105**, 168101 (2010).

[29] Campbell, N. The study of discontinuous phenomena. In *Proc. Camb. Philos. Soc.*, vol. 15, 117–136 (1909).

[30] Mantegna, R. N. & Stanley, H. E. Stochastic process with ultraslow convergence to a Gaussian: the truncated Lévy flight. *Phys. Rev. Lett.* **73**, 2946 (1994).

[31] Wang, B., Kuo, J., Bae, S. C. & Granick, S. When Brownian diffusion is not Gaussian. *Nature Mater.* **11**, 481–485 (2012).

[32] Chechkin, A. V., Seno, F., Metzler, R. & Sokolov, I. M. Brownian yet non-Gaussian diffusion: From superstatistics to subordination of diffusing diffusivities. *Phys. Rev. X* **7**, 021002 (2017).

[33] Viswanathan, G. M. *et al.* Optimizing the success of random searches. *Nature* **401**, 911 (1999).

[34] Humphries, N. E., Weimerskirch, H., Queiroz, N., Southall, E. J. & Sims, D. W. Foraging success of biological Lévy flights recorded in situ. *Proc. Natl. Acad. Sci.* **109**, 7169–7174 (2012).

[35] Bénichou, O., Loverdo, C., Moreau, M. & Voituriez, R. Intermittent search strategies. *Rev. Mod. Phys.* **83**, 81 (2011).

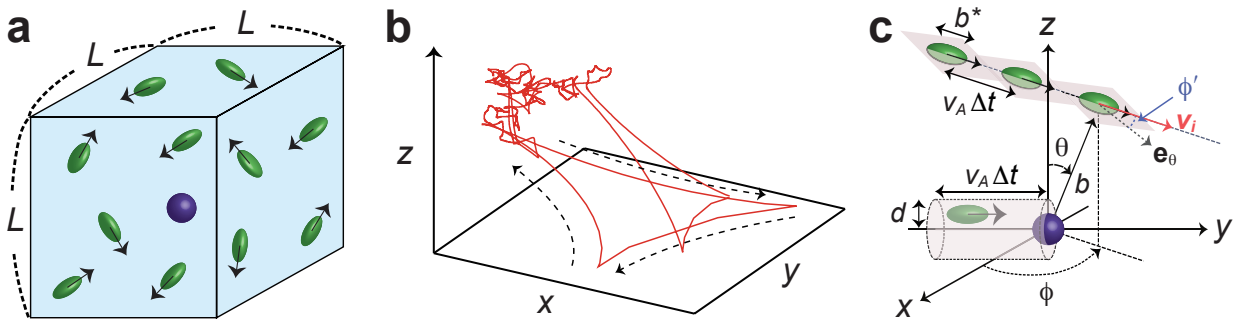

FIG. 1. **Illustration of the microscopic model.** (a) Active swimmers (green ellipsoids) and a passive tracer (violet sphere) are suspended in a cubic box of edge length L. The direction of the swimmers $\mathbf{n}_i \equiv (\sin\theta_i \cos\phi_i, \sin\theta_i \sin\phi_i, \cos\theta_i)$ is randomized upon hitting the box boundary. We consider a sufficiently large box $L \to \infty$ under the dilute condition $\rho d^3 \ll 1$, where $\rho \equiv m/L^3$, and set length and time units as $b^* = 1$ and $\tau_\mathrm{H} \equiv b^*/v_\mathrm{A} = 1$ (see SI Sec. I for protocol details). (b) Typical simulated tracer trajectory exhibiting characteristic non-closed loops for pusher swimmers ($p < 0$, $d = b^*$). (c) Two exemplary swimmer–tracer interaction events. Top: a two-body scattering event with impact parameter $b > d$ and injection angles θ, ϕ, and ϕ', with the unit vector $\mathbf{e}_\theta$. Bottom: a collision event with $b \leq d$. A swimmer travels the distance $v_\mathrm{A}\Delta t$ in a time interval Δt. We define the time at which this distance is equal to the characteristic length scale b^* as τ_H. Since b^* is related to the typical length scale of a swimmer, for $\Delta t \ll \tau_\mathrm{H}$ the motion of the swimmers can be effectively neglected (see SI, Fig. S3). Conversely, for a given set of injection angles swimmers can collide against the tracer in the time interval Δt if they are contained in a cylinder with cross section area πd^2 and length $v_\mathrm{A}\Delta t$ surrounding the tracer. The mean free time of the tracer τ_C is then estimated as $\rho\pi d^2 v_\mathrm{A}\tau_\mathrm{C} = 1, i.e., \tau_\mathrm{C} \equiv 1/(\rho v_\mathrm{A}\pi d^2)$. For $\Delta t \ll \tau_\mathrm{C}$ such collision events do not contribute to the tracer dynamics.

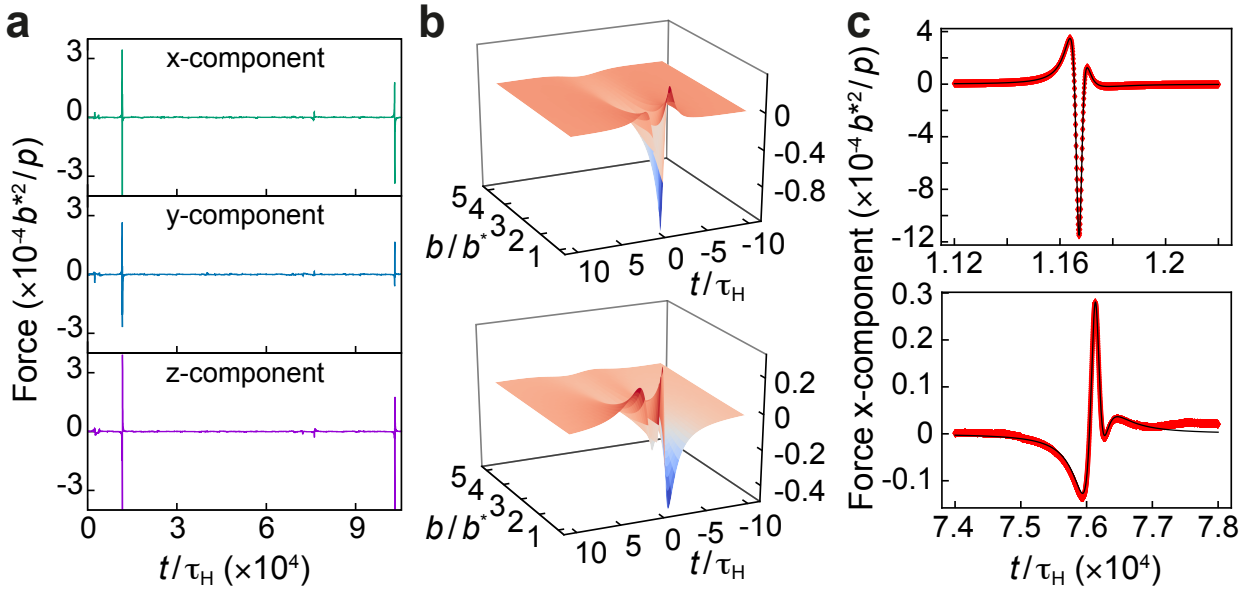

FIG. 2. **The force exerted on the tracer by the swimmers.** (a) Typical time series in the simulation ($p < 0$, $d = b^*$). (b) 3D plots of the projected FSF $f_{\mathbf{b}}(t) \equiv \mathbf{e}_x \cdot \mathbf{f}_{\mathbf{b}}(t)$, which is characterized by the parameter set $\mathbf{b} \equiv (b, \theta, \phi, \phi')$. We consider $\{\theta, \phi, \phi'\} = \{\pi/2, 0, \pi/2\}$ (top panel) and $\{\theta, \phi, \phi'\} = \{0, 0, 0\}$ (bottom panel). These two special cases form a base representation of the general solution for $f_{\mathbf{b}}(t)$ up to 2nd order (see SI Sec. II D). (c) Exemplary fits (black solid line) of $f_{\mathbf{b}}(t)$ to simulation data of two scattering events arbitrarily extracted from the force time-series (a). Fit parameters are $\mathbf{b}$ and τ, which are obtained using nonlinear least squares (see SI Sec. II D).

ACKNOWLEDGMENTS

We appreciate D. Mizuno, H. Takayasu, M. Takayasu, H. Hayakawa, and F. van Wijland for fruitful discussions. This work was supported by Grant-in-Aid for JSPS Fellows (Grant No. 16J05315), JSPS KAKENHI (Grant Nos. 16K16016 and 18K13519), the Research Fellowship granted by the Royal Commission for the Exhibition of 1851, and Atoms program granted by the Yukawa Institute for Theoretical Physics. The numerical calculations were carried out on XC40 at Yukawa Institute for Theoretical Physics in Kyoto University.

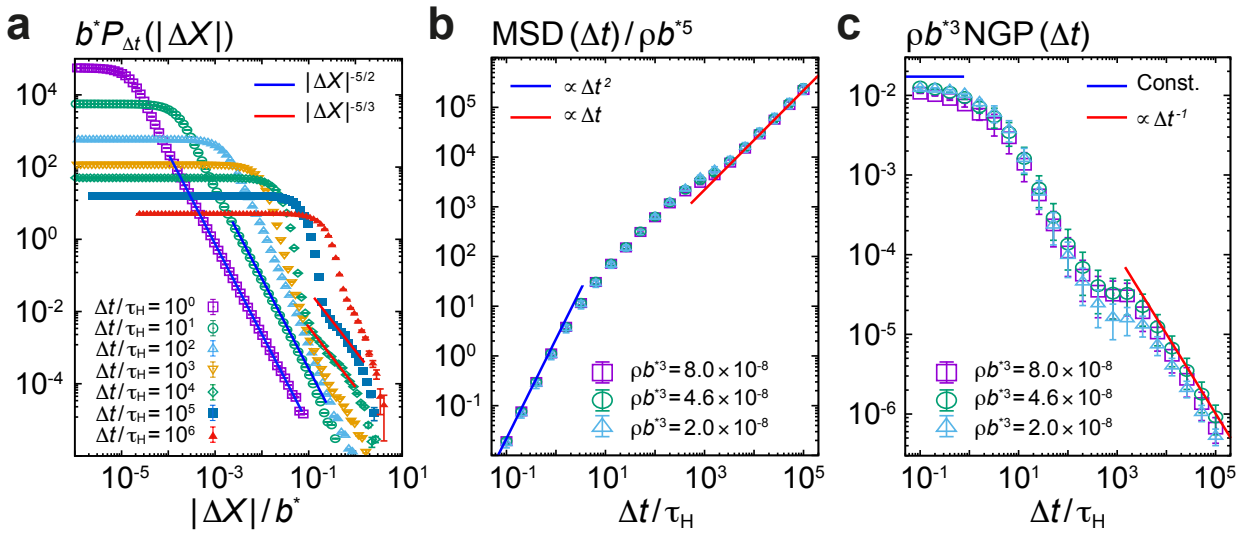

FIG. 3. **Simulation results confirming the theoretical predictions.** (a) The PDF $P_{\Delta t}(|\Delta X|)$ of the tracer displacements ΔX exhibiting power-law tails and the reversal to a Gaussian for large Δt. The crossover scaling from $\alpha_{\rm H} = 5/2$ to $\alpha_{\rm S} = 5/3$ should be experimentally testable (see SI Sec. V). (b) Data collapse of MSD$(\Delta t) \equiv \langle \Delta X^2 \rangle$ upon rescaling by $1/(\rho b^{*5})$ exhibiting a crossover between ballistic and normal diffusive motion [3, 4, 6, 7, 10]. (c) Data collapse of NGP$(\Delta t) \equiv \langle \Delta X^4 \rangle / (3\langle \Delta X^2 \rangle^2) - 1$ upon rescaling by ρb^{*3} exhibiting a power-law decay Δt^{-1} for large Δt [10]. Error bars denote ± 1 s.e.m..

AUTHOR CONTRIBUTIONS

KK, TGS, AC, and AB designed the research and interpreted results. KK and AC performed analytical calculations. TGS performed numerical simulations. AB managed the project. KK, AC, and AB wrote the paper.

COMPETING INTERESTS

The authors declare no competing financial interests.

DATA AND CODE AVAILABILITY

Simulation data were generated at XC40 at Yukawa Institute for Theoretical Physics in Kyoto University. Derived data supporting the findings of this study are reproducible by the simulation code, available at https://doi.org/10.5281/zenodo.3550834. The time series data used in Fig. 1b and Fig. 2b are accessible as a text file at https://doi.org/10.5281/zenodo.3550838. The further data will be available from Tomohiko G. Sano upon request.